Adhesive forces between two cleaved calcite surfaces in NaCl solutions: The importance of ionic strength and normal loading
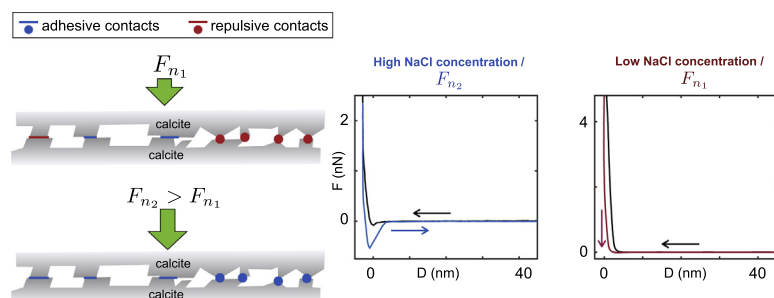
Shaghayegh Javadi [a,c,b,*], Anja Røyne [b]

[a] The National IOR center of Norway, University of Stavanger, Norway
[b] Department of Physics, University of Oslo, Norway
[c] Department of Energy Resources, University of Stavanger, Norway

GRAPHICAL ABSTRACT

ARTICLE INFO

ABSTRACT

The mechanical strength of calcite bearing rocks is influenced by pore fluid chemistry due to the variation in nano-scale surface forces acting at the grain contacts or close to the fracture tips. The adhesion of two contacting surfaces, which affects the macroscopic strength of the material, is not only influenced by the fluid chemistry but also by the surface topography. In this paper, we use Atomic Force Microscope (AFM) to measure the interfacial forces between two freshly cleaved calcite surfaces in $CaCO_3$-saturated solutions with varying NaCl concentration. We show that calcite contacts become stronger with increasing NaCl concentration (>100 mM), as a result of progressively weaker secondary hydration and increasing attraction due to instantaneous ion-ion correlation. Moreover, we discuss the effect of normal applied force (F_n) and surface roughness on the measured adhesion forces (F_{ad}). We show that the measured pull-off force (adhesion) is linearly correlated with the magnitude of F_n, where an increase in applied force results in increased adhesion. This is attributed to a larger number of contacting surface asperities and thus increase in real contact area and the contact-bond strength. We discuss that the possible variation in local topography at contacts, together with strong dependence on ionic strength of the solution, can explain the inconsistent behavior of calcite rocks in NaCl solutions.

© 2018 Elsevier Inc. All rights reserved.

1. Introduction

Calcite is an abundant mineral in nature. It is a crystalline polymorph of calcium carbonate with a cleavage plane along the $(1\,0\,\bar{1}\,4)$ direction [1–3]. Calcite plays a key role in biomineralization and it is a constituent of shells and skeletons of many marine

---

invertebrates [4]. Moreover, it is one of the most common rock-forming minerals of importance to hydrocarbon recovery, CO_2 sequestration [5,6] and nuclear waste storage [7]. Calcite is the main constituent mineral of chalk (>99%). Chalk deposits form many of the world's oil and gas reservoirs, such as the North Sea oil reserves, where they alone account for 25 million barrels of oil since the 1970s [8].

Chalk reservoirs are prone to strong compaction, due to water injection associated with Enhanced Oil Recovery (EOR) projects [9–13]. The mechanical behavior of chalk and calcite-bearing rocks is known to be influenced by the pore fluid chemistry [9,14–17], an effect that is often referred to as water-weakening (the significant loss of mechanical strength of chalk in water-saturated rocks [12,18]). Several mechanisms have been proposed to describe this phenomenon, such as pressure solution [19,20], chemical influences [19], invading the capillary bridges/menisci by water flooding [21], time-dependent water adsorption on calcite surfaces [11,22] and subcritical crack growth at the grain boundaries [23]. In the early 2000s, Risnes et al. [12,18] proposed that water activity is a key parameter behind the strength loss in chalk in aqueous solutions. Hellmann et al. [13] suggested that water-weakening may be also related to the repulsive forces due to adsorbed water molecules on adjacent calcite surfaces. These two hypotheses were further supported by atomic force microscope (AFM) experiments by Røyne et al. [24], in which adhesion between two surfaces depended on water activity, with strong repulsion measured in pure water.

At the nano-scale, repulsive and attractive forces operate between two calcite surfaces that are separated by a thin fluid film. Surface forces between two charged surfaces in an electrolyte solution can be described by the Derjaguin-Landau and Verwey-Overbeek (DLVO) theory [25,26] that includes van der Waals (vdW) and Electrical Double Layer (EDL) forces [27,28]. However, at separations significantly shorter than the Debye length, and for solutions with high ionic strength (>0.1 M) [28,29], where specific ion interactions and hydration effects become exceedingly important, [30–36] the DLVO theory cannot accurately describe the interaction between surfaces in aqueous solutions. The AFM direct force measurements by Røyne et al. [24] shows that the observed repulsion in water is due to hydration forces acting between two hydrophilic calcite surfaces. A similar experiment by Pourchet et al. [37] indicates that attractive forces act between calcite surfaces in high pH and higher ionic strength solutions (0.12 M), which were attributed to the ion-ion correlation forces. Both hydration and ion-correlation forces are not included in the DLVO theory.

Several studies have shown that the degree of water weakening is also affected by the salinity of the pore fluid [12,18,38]. The salinity of the solution affects both the EDL component of the DLVO forces, and the water activity [39,40]. It also changes the calcite dissolution kinetics in aqueous solutions [41–44].

In general, calcite and other natural mineral surfaces display some degree of roughness at a molecular scale. Several studies have shown that surface roughness affects the water wettability of calcite [45,46] and oil desorption from calcite surfaces [47]. It, also, influences the interfacial forces between mineral surfaces in molecular scale. This is because of the actual contact area is always smaller than the nominal surface area (see Fig. 1) [48–57]. For rough surfaces, contacting surface asperities give rise to an exponentially decaying repulsive force upon loading [58], which can potentially be interpreted as hydration repulsion, as in the past studies [58,59].

Calcite surfaces are dynamic in aqueous solutions, with continuous dissolution and recrystallization on the timescale of hours even in saturated solutions, as shown by Stipp et al. [60,61]. We, therefore, expect the distribution and geometry of surface asperi-
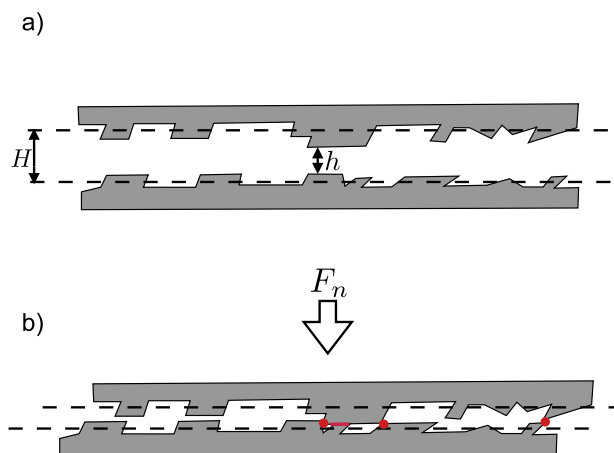

Fig. 1. A simple sketch of two opposing, cleaved calcite surfaces with nano-scale roughness characterized by steps and terraces on the (1 0 1 4) surface. (a) Dotted lines represent the midline of surface asperities with H as the surface separation, and "h" is the distance between highest asperities. (b) When two surfaces pushed into contact by an applied normal load (F_n), a discrete number of asperities are forced into contact, as represented by the red dots and lines. The sum of these discrete areas of contact are referred to the actual area of contact for rough, contacting surfaces. (For interpretation of the references to color in this figure legend, the reader is referred to the web version of this article.)

ties to change with time, which in turn influence the magnitude of repulsive mechanical effects due to asperity deformation. Recently Dziadkowiec et al. [62] performed force measurement experiments between two rough calcite surfaces (with nm-scaled asperities), using the Surface Force Apparatus (SFA). They observed repulsive forces with a decay length that increases with time, which was explained by repulsive hydration forces combined with continuous recrystallization and roughening of the calcite films in saturated $CaCO_3$ solutions.

The effect of NaCl on the interaction between calcite surfaces is of interest because both Na^+, and Cl^- are the two most abundant monovalent ions in seawater. The influence of NaCl on the strength of carbonate rocks [15,16,63] and EOR systems has been extensively investigated in surface science and reservoir engineering, e.g. [64–66]. Liu et al. [64] observed that injection of NaCl solution (low and high concentrations) into a carbonate rock increases the oil desorption rate from calcite surfaces. They explained this result by increased solubility of calcite in high concentration NaCl solution, which in turn increases the local pH, leading to more negatively charged calcite surfaces and hence repulsive forces between the calcite and the oil. For low NaCl concentrations, they relate the high-rate oil desorption to the EDL repulsive forces between oil and calcite surfaces. Interestingly, in contrast, Fathi et al. [65,66] showed that oil recovery improves when the NaCl (named as non-active salt) is removed from the seawater. This effect was attributed to a high population of Na^+ and Cl^- near the calcite surfaces that prevents the potential determining cations/anion (Mg^{2+}, Ca^{2+} and SO_4^{-2}) to reach to the surface. As a result, a more positively charged calcite surface attracts oil to a higher extent. However, they show that surface reactivity and ultimately wettability of the surface varies with the temperature as well as the solution ionic strength. This shows the increased complexity of the calcite-brine-calcite system once the oil is present. In fact, the type and history of mineral surfaces, and the components of oil and brine are inevitable parameters and shall thus be considered when investigating such a system.

In this study, we aim to understand the role of ionic strength in compaction of calcite-bearing rocks, and its potential relation to the nm-range forces between calcite surfaces. To achieve this, we use the colloidal probe AFM with a calcite probe against a freshly

cleaved calcite surface. We investigate the pull-off force between two calcite surfaces, as a measure of the adhesion and surface energy between two surfaces, [41,67] in NaCl solutions with concentrations ranging from 1 mM to 1.2 M, pre-saturated with calcium carbonate. We additionally address, indirectly, the effect of applied normal force (F_n) on the pull-off forces and its relation to intrinsic roughness of natural cleaved calcite surfaces.

2. Experimental method

2.1. Force measurement using AFM

To measure forces between two calcite surfaces we use a JPK NanoWizard® 4 Bioscience AFM, in force spectroscopy mode. The AFM is situated on an inverted Olympus IX71 microscope. The approach and retract velocities are set to 200 nm/s, where we observe negligible hydrodynamic effects. The maximum applied normal load, or set point (Fig. 2), is varied from 5 to 30 nN in steps of 5 nN. For each approach-retract curve, we record one value for the pull-off (adhesion) force (Fig. 2). The temperature inside the AFM enclosure is continuously monitored, and found to be stable at 24.5 ± 0.5 °C.

2.2. Sample preparation

2.2.1. Calcite surface and fluid cell

Each experiment is performed with a freshly cleaved Iceland spar calcite crystal. A 5 × 5 mm crystal is first glued to a glass slide using a UV-curing adhesive (Casco Glaslim) and cleaved *in situ*. To make the fluid cell, we use a plastic ring (20 mm inner diameter, 6.5 mm height, final capacity approx. 3.5 ml) with inlet and outlet ports connected to plastic tubing, and fix it around the sample using a self-cure rubber (Reprorubber). The fluid cell is loosely sealed at the top by a silicone membrane to reduce the fluid evaporation rate. Fig. 3a–c show the production of calcite probe and assembling the fluid cell (with calcite crystal in) on the AFM stage.
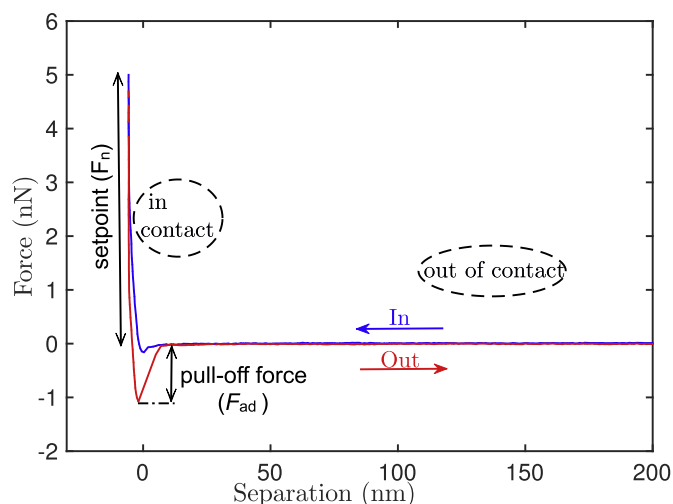

Fig. 2. One representative force curve measured in 800 mM NaCl solution, with setpoint F_n = 5 nN. The approach curve (blue line) shows a sudden small vdW attraction at short distance, and repulsion closer to or at the contact. The measurement shows a characteristic jump-out upon retraction (red line) and the minimum value of this curve, called the pull-off force, is used as a measure of the adhesive interaction of the surfaces. The non-contact area shows the force zero line obtained by fitting a straight line to the corresponding data points of the cantilever deflection versus piezo position curve. In this description, some terminologies are used from [24,68]. (For interpretation of the references to color in this figure legend, the reader is referred to the web version of this article.)

2.2.2. AFM-probe modification

We adapt the method described by [24] (see Fig. 3a–b) for AFM-tip fabrication. A suitable calcite fragment (size between 40–70 μm in length and 15–25 μm in width) is identified under the microscope. A tipless cantilever (All In One-TL, 15 kHz, 0.2 N/m) is moved over a drop of two component epoxy glue (Epoxy Universal 335, DANA LIM, mixing ratio 1:1), picks it up and moves back to the position of the chosen particle. The cantilever is then brought into contact with the particle and left at a constant applied force overnight to set (12–16 h). In order to ensure two parallel interacting surfaces, all measurements are made without moving the particle from its initial position. Before each gluing process, we measure the spring constant of the cantilever using the thermal tune calibration method [69]. In addition, we measure the cantilever sensitivity using a contact based force-distance curve, after each solution injection.

2.2.3. Solutions

Solutions are made using various concentrations of NaCl (VWR, 100.2%) (see Table 2) in deionized (type II) water. All solutions are saturated with $CaCO_3$ (excess powder of $CaCO_3$ in deionized water). The $CaCO_3$ powder (MERCK) is heat treated at 300 °C in a clean laboratory environment to minimize any possible organic contamination. All solutions are shaken and left stationary for at least 2 weeks to equilibrate. Before each measurement, we place the vials containing the solutions inside the AFM enclosure for at least 12 h, for thermal equilibration. The pH of each solution is measured before and after the experiment (see Table 1), and shows no significant change. We compare these results with pH-values calculated using PHREEQC [70], for open systems (OS) in equilibrium with atmospheric CO_2 (log(pCO_2) = −3.5), and for closed systems (CS) with no exchange of CO_2 with the atmosphere. Most of the measured values are between those calculated for OS and CS. This shows that the equilibrium with atmospheric CO_2 and calcite had not been fully reached; however, since the pH did not change during the measurement, we do not expect this process to influence our results. We also calculate the equilibrium Ca^{2+} concentration and find it to be of negligible influence on the ionic strength for NaCl concentrations higher than 5 mM.

2.3. Procedure

Once the calcite probe is fabricated, we start the experiment by performing a few force measurements in air, and then injecting the first solution (see Fig. 4 for the workflow of a typical experiment). We allow the system to equilibrate for 15 min after each fluid injection. To separate the effect of salt concentration and elapsed time, we inject the solutions in random order. Experiments continue for at least 10 h unless they have to be aborted because of a lost particle during measurement, or a piece of dust becomes permanently trapped between the surfaces after fluid injection. The AFM probe is stored in a sealed container after each successful measurement to be imaged by a Scanning Electron Microscope (SEM, TM3030Plus), after no more than one week (Fig. 3d-left). The results of EDS analysis do not show any precipitation of secondary minerals on these surfaces. We, also, use a white light interferometer (WLI) optical profiler (GTK-contour Bruker) to measure the topography of the calcite probes. Each surface is characterized by steps and terraces and the rms-values (root mean squared) indicate the height differences between microscopic terraces over the total surface area (see Fig. 3d for the SEM and WLI scans of a representative particle).
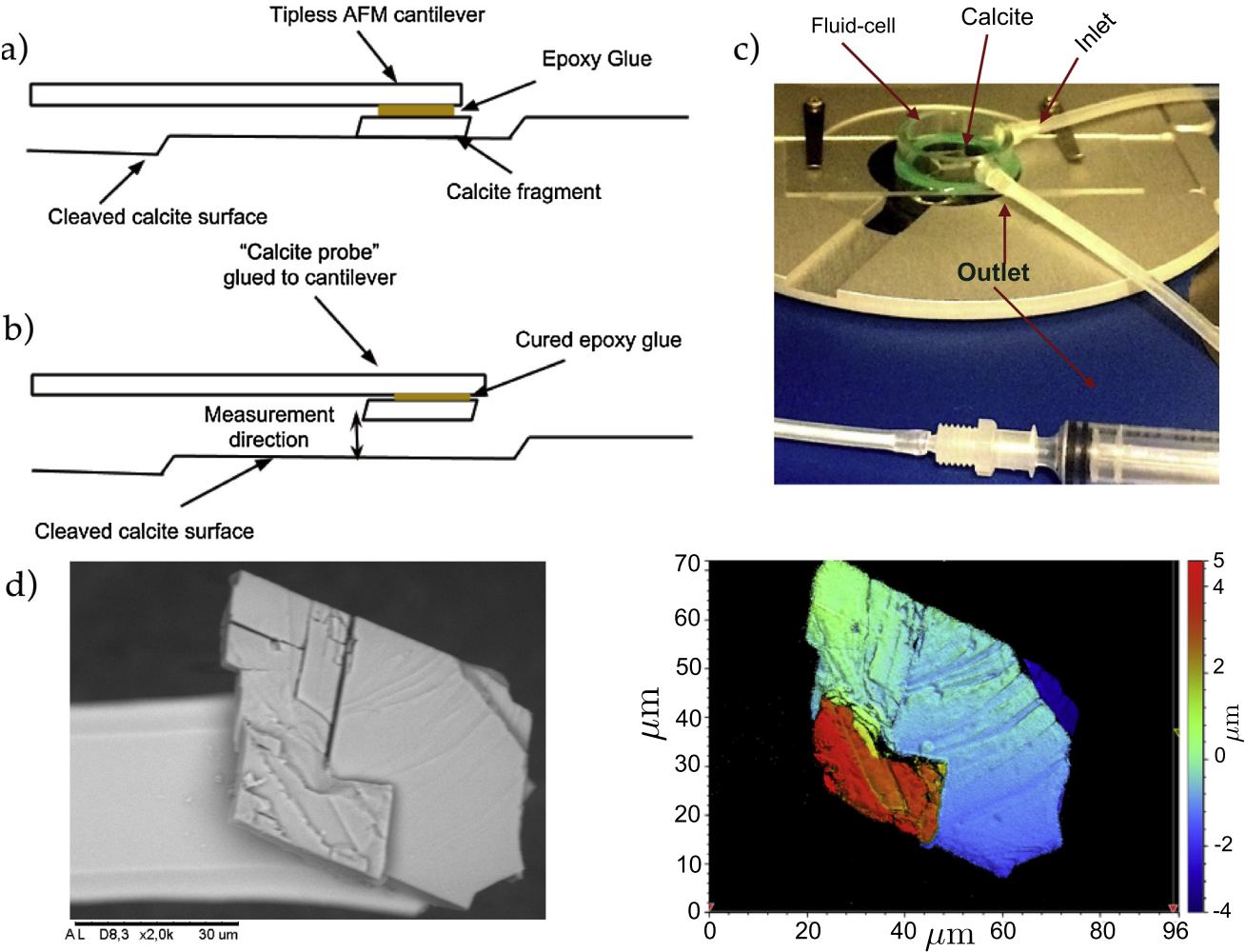
Fig. 3. AFM-tip modification procedure. (a) Freshly cleaved calcite crystal with small fragment on surface, and cantilever with a drop of Epoxy glue is about to be in contact. (b) After 16 h the cured Epoxy glue yields attached particle to cantilever. By separating them from the surface, we can start the measurement. (c) AFM-stage with a mounted fluid cell containing a cleaved calcite ready for the tip-fabrication process. Fluid exchange happens through the inlet/outlet tubes. (d-left) SEM image of a representative particle, after the experiment, with rms = 583 nm over A = 1352 μm^2. (d-right) WLI scan showing the surface topography of the same particle.

Table 1
Measured pH after the experiment (with ±0.1 deviation for all used solutions) and PHREEQC simulation results for open (OS) and closed systems (CS). The equilibrium concentration of Ca^{+2} is also calculated by PHREEQC in both OS and CS. The ionic strength for the highest concentration is calculated as 1290 mM (including Ca^{+2} and CO_3^{-2}).

NaCl (mM)	Measured pH(after exp. in OS)	Calculated pH (CS)	Calculated pH (OS)	Calculated Ca^{2+}(OS) (mM)	Calculated Ca^{2+}(CS) (mM)
0	9.00	9.91	8.27	0.48	0.12
1	8.96	9.91	8.28	0.49	0.13
2	8.42	9.91	8.28	0.50	0.13
3	9.03	9.91	8.28	0.51	0.14
4	8.38	9.91	8.29	0.52	0.14
5	8.36	9.91	8.29	0.54	0.14
10	8.27	9.92	8.30	0.56	0.15
20	8.50	9.92	8.31	0.60	0.17
30	8.16	9.92	8.32	0.63	0.19
40	8.67	9.92	8.33	0.66	0.20
50	8.14	9.92	8.33	0.68	0.21
100	8.87	9.92	8.35	0.76	0.26
200	8.00	9.91	8.36	0.87	0.34
300	8.09	9.90	8.36	0.96	0.40
400	8.50	9.89	8.37	1.02	0.45
500	8.22	9.88	8.36	1.07	0.49
600	8.34	9.87	8.36	1.11	0.53
700	8.23	9.86	8.36	1.15	0.56
800	9.78	9.86	8.35	1.18	0.58
900	8.75	9.85	8.35	1.21	0.60
1000	9.80	9.85	8.35	1.23	0.63
1100	7.86	9.84	8.34	1.25	0.65
1200	8.23	9.84	8.34	1.27	0.66

Table 2
List of particles, used solutions (shown by marker (×)), measured surface area by optical camera before experiment (A_{op}) and SEM after the experiment (A_{SEM}) and measured roughness (rms) by white light interferometer (WLI) for each particle. There is no information on A_{SEM} and rms for particles that were lost at the end or during the experiment. Zero value for NaCl concentration represents a saturated $CaCO_3$ solution only.

P (#)	A_{op} (µm²)	A_{SEM} (µm²)	rms (nm)	0	1	2	3	4	5	10	20	30	40	50	100	200	300	400	500	600	700	800	900	1000	1100	1200
1	918	788													×	×	×	×	×	×	×	×	×	×	×	×
2	2562	1242												×	×	×	×	×	×	×	×	×	×	×	×	×
3	1905													×	×	×	×	×	×	×	×	×	×	×	×	
4	564													×	×	×	×	×	×	×	×	×	×	×	×	×
5	1099				×	×	×	×	×	×	×	×	×	×	×												
6	650	499	443		×	×	×	×		×	×		×	×	×			×	×			×		×		×
7	1195	958	761	×	×			×	×		×	×		×	×		×			×		×		×		×
8	693	708		×		×	×						×		×		×			×				×		
9	1489	1017	931	×	×			×	×		×			×	×		×		×		×		×		×	

3. Results

The measured pull-off forces (F_{ad}) from all experiments are summarized in Fig. 5, plotted as cumulative distributions for each concentration and particle (p_1 - p_9), where the results of different applied forces are plotted as different colored lines. Each panel is marked with a number representing the order of fluid injections (t_i, where $i = 1, 2, \ldots, 14$).

3.1. Effect of NaCl concentration

As seen in Fig. 5, the general trend for each experimental day (particle) is that the measured pull-off forces increase with increasing concentration of NaCl. At low concentrations (below
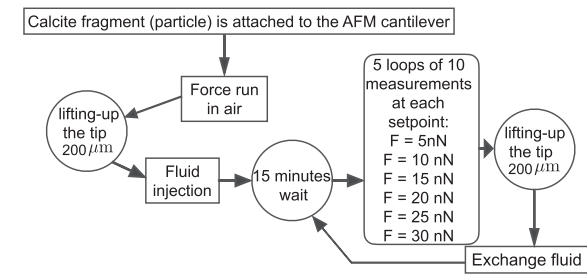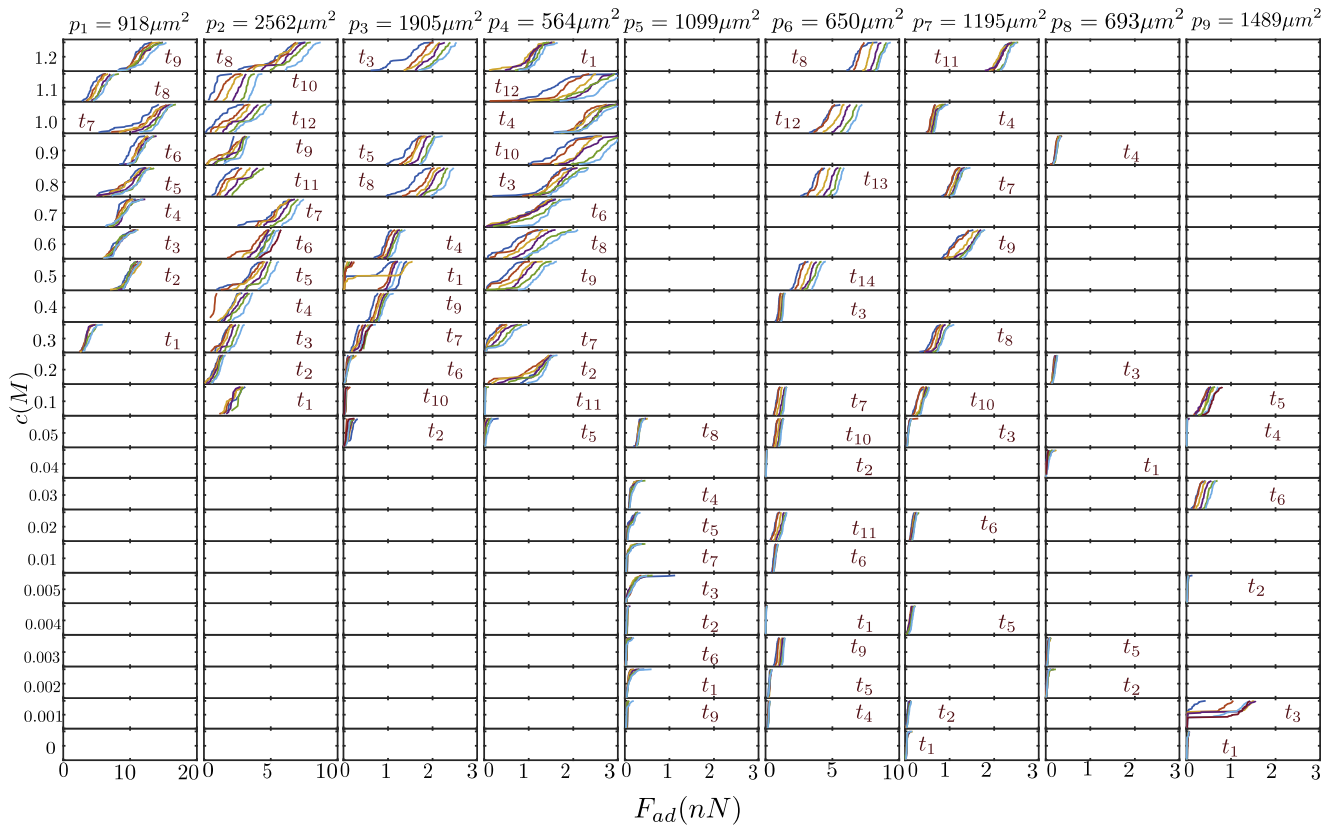

Fig. 4. Flowchart of the experimental procedure.

Fig. 5. Cumulative measured adhesion for all experimental days and salt concentrations. y-axis stands for experimental NaCl concentration and x-axis for measured adhesion, whose limitation depends on the maximum measured F_{ad} for each day. Different colors show the measured values at different applied force (F_n). In these plots, t_i represent the injection order, where $i = 1, 2, \ldots, 14$. (For interpretation of the references to color in this figure legend, the reader is referred to the web version of this article.)

100 mM), F_{ad} is either zero or very low in almost all measurements, consistent with the observations of Røyne et al. [24]. At higher concentrations, F_{ad} is non-zero in all cases.

In some experiments, the increase in F_{ad} with concentration is not monotonic. Abrupt changes in F_{ad} can take place when the solution is exchanged. This is clear, in Fig. 5, for particle p_2, where F_{ad} is reduced from t_7 (0.7 M) to t_9 (0.9 M) and then behaves the same for the rest of the measurements. We believe that these sudden changes can be caused by lateral movement of the cantilever [67] relative to the cleaved surface, or, less likely, by surface contamination (small particle(s) of calcite or other dust) getting caught between the surfaces, undetected by the subsequent force curves.

3.2. Effect of applied force

As seen in Fig. 6, for all experiments, the measured pull-off force increases with increasing applied normal stress. This behavior can be fitted, for all experiments, to a linear function of the form,

$$F_{ad} = \alpha F_n + F_{ad}^0 \qquad (1)$$

where F_{ad} is the measured pull-off force and F_n is the setpoint (applied normal force). Fig. 6 shows the results of all experiments collapsed onto a single curve by rescaling with the fitted parameters, where the slope of the fitting curve increases between 0.01 and 0.19, independently of concentration (Fig. 6, top-left inset).

3.3. Effect of time

Given that calcite surfaces are known to be dynamic in aqueous solutions [71], with continuous dissolution and recrystallization at the nano-scale, we expect that the actual area of contact (the sum of discrete nano-asperities) could change through time. Since the measured pull-off forces reflect the number of asperities in contact, we can detect such variation by looking at a possible gradual change in measured pull-off forces as a function of time. Fig. 7 shows the result of F_{ad} for p_6 in 500 mM NaCl solution. Each of the clusters represents the measured F_{ad} values in each loop (following the procedure as shown in Fig. 4), where the results of different F_n are plotted in different colored circles. We observe a slow change with time in F_{ad} for each F_n. However, there is no consistent trend: sometimes we see increase in F_{ad} with time, sometimes

Fig. 7. Measured adhesion with time for p_6 in 500 mM NaCl solution. Adhesion forces increase by F_n in each loop, and mostly return to their initial state (at low value of F_n) for the next loop.

decrease. The trend can change from increasing to decreasing or vice versa.

3.4. Effect of particle size

Fig. 8 shows the measured pull-off force for 6 different particles at three values of applied force, F_n = 5, 20 and 30 nN in NaCl concentration of 1200 mM. There is no clear correlation between nominal particle area and measured pull-off force, indicating that surface roughness and actual area of contact, are more important parameters than the nominal surface area. Note that this result is independent of the fluid composition and setpoint values.

We could expect that the magnitude of the pull-off force in air would be a measure of the actual area of contact, which would mean that normalizing by the adhesion in air, should give a measure of adhesive energy per unit area. However, this normalization does not reduce the variation in adhesion values for different particles for any given salt concentration nor setpoint. This is probably because the pull-off force in air is dominated by the breaking of
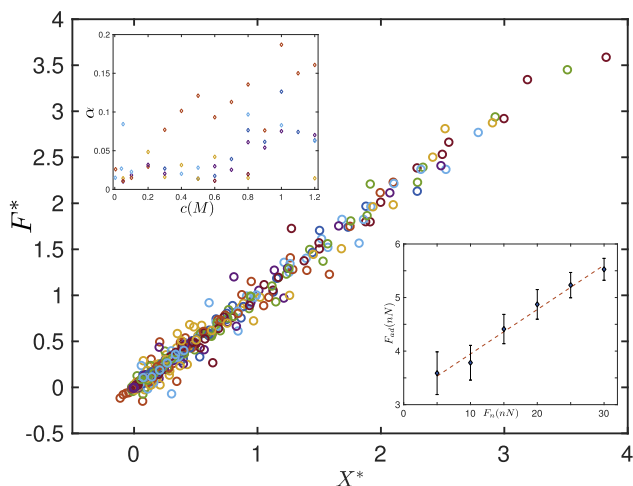
Fig. 6. Data collapse of pull-off force vs. applied normal load, for all experiments, with $X^* = \alpha F_n$ and $F^* = F_{ad} - F_{ad}^0$. The insets represent, (top-left) the slope (α) of the fitting curve vs. concentration (x-axis is plotted in logarithmic scale), and (right-bottom) a representative result for p_6 in NaCl 800 mM solution.
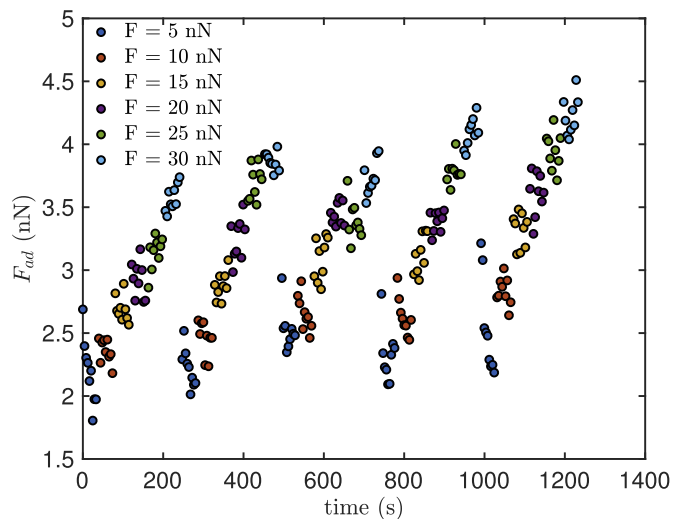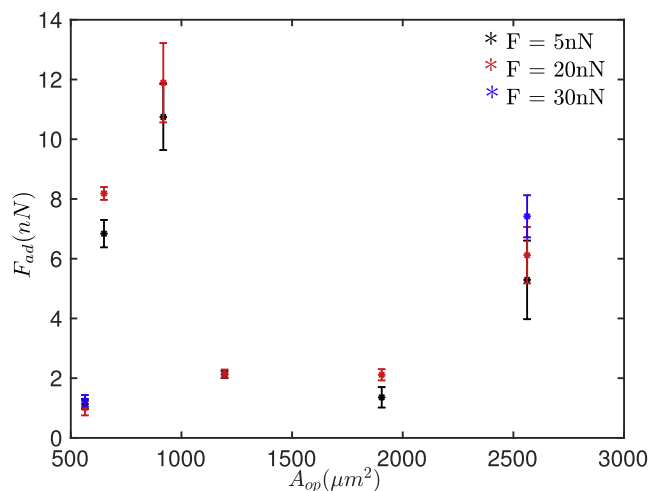
Fig. 8. We see no correlation between pull-off force and surface area. This plot shows the measured pull-off force vs. surface area (optical measured values) for different particles in 1200 mM NaCl solution at 3 different values for F_n.

capillary bridges, which is more influenced by the specific contact geometry than the actual area of contact.

4. Discussion

Our results can be summarized as follows: (1) the interactions between calcite surfaces goes from repulsive to adhesive at NaCl concentrations around 100 mM, and the adhesive interaction (pull-off force) increases with salt concentration; (2) for adhesive interactions, pull-off forces increase with increasing applied normal load; and (3) the pull-off forces change slightly with time in a non-monotonic fashion.

When two surfaces are in an electrolyte solution, the interaction potential between them determines the compressive force necessary to push them into adhesive contact. Fig. 9 shows the disjoining pressure, force per area for two flat calcite surfaces, given by DLVO theory as the sum of van der Waals (vdW) and electric double layer (EDL) forces [28]:

$$F_{vdW} = -\frac{A}{6\pi D^3} \quad \text{and} \quad F_{EDL} = \left(\frac{\lambda^2}{2\pi}\right) Z e^{-\lambda D} \qquad (2)$$

where λ is the Debye length and Z is the interaction constant calculated by $Z = 64\pi\epsilon_0\epsilon(kT/e)^2 \tanh^2(e\psi_0/4kT)$ [28]. ψ_0 is the surface potential and a function of the pH of solution, Ca^+ concentration [43,44] and P_{CO_2} [72]. For a monovalent electrolyte, Z differs between 1.95×10^{-18} and 3.47×10^{-18} J m^{-1}, where ψ_0 is expected to vary between 15 and 20 mV throughout the experiment for pH between 8 and 9 [72, Figure B]. A is the non-retarded Hamaker constant, calculated based on Lifshitz theory through [28],

$$A = \frac{3}{4}kT\left(\frac{\epsilon_1 - \epsilon_3}{\epsilon_1 + \epsilon_3}\right)^2 + \frac{3h\nu_e}{16\sqrt{2}}\frac{(n_1^2 - n_3^2)^2}{(n_1^2 + n_3^2)^{3/2}}$$

where $n_1 = 1.48$ and $\epsilon_1 = 8$ are refractive index and dielectric permittivity of calcite [29], and $n_3 = 1.33$ and $\epsilon_3 = 80$ are the refractive index and dielectric permittivity of water. $h = 6.6 \times 10^{-34}$ m^2 kg/s is the Planck constant and $\nu_e = 3 \times 10^{15}$ s^{-1} is the main electronic absorption frequency in the UV [28]. In general, the DLVO interaction energy is affected by the ionic strength of the electrolyte solution [53]. Increasing salt concentration, changes the position and height of EDL repulsive barrier. As the salt concentration increases,
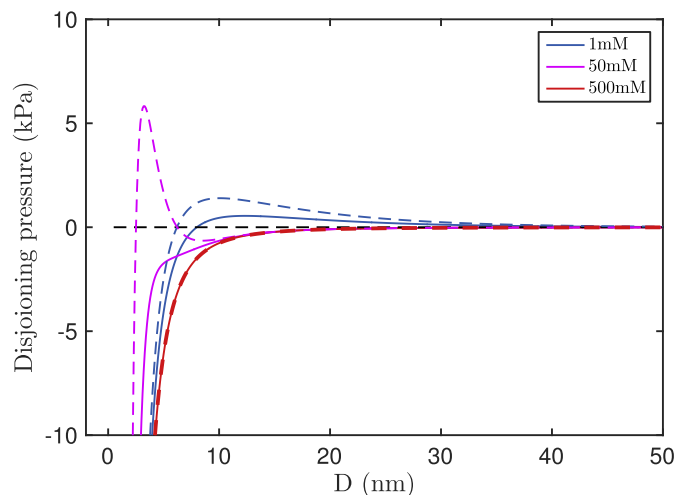

Fig. 9. Calculated DLVO for two flat, smooth calcite surfaces in NaCl solution with a few values of ionic strength, Eq. (2). It shows a higher repulsive barrier by reducing the Debye length and its diminishing effect at low values. Dotted lines: for $\psi_0 = 20$ mV, and Solid lines: for $\psi_0 = 15$ mV.

the van der Waals attractive forces contribution overcomes the EDL repulsive forces (Fig. 9).

At first glance, this could explain the increased adhesion we see at high salt concentration. However, two observations do not fit this hypothesis: (1) as noted by Røyne et al. [24], the magnitude of the EDL repulsive barrier for calcite surfaces in low ionic strength solution is very small, and unlikely to explain the purely repulsive behavior observed under these conditions; and (2) the observed pull-off forces increase in magnitude even as the ionic strength is increased beyond what should be the limit of the DLVO theory [29,31,48,73–75].

An increase in the measured pull-off force can be explained by a decrease in any repulsive barrier present (due to EDL or hydrophilic repulsion), to an increase in the adhesive interaction (van der Waals or ion correlation forces), or both.

It has been suggested by Blandamer et al. [40] that water activity, which is known as the effective mole fraction of water (a_w), defined by the product of activity coefficient (γ_w) times by mole fraction of water (x_w) in that solution, $a_w = \gamma_w x_w$, controls water adsorption and thereby hydrophilic repulsion. By increasing the concentration of ions in solutions, water molecules become more involved with ion-dipole interactions in the bulk fluid that gives rise to hydrated ionic species. This affects surface water absorption on both hydrophilic surfaces, and results in less required force to make adhesive contacts due to the decrease in both magnitude and onset of the hydration forces [50]. Risnes et al. [12] and Rostom et al. [38] also showed that the strength of carbonate rocks and fracture threshold of calcite are affected by the salinity level of pore fluid and attributed this to the level of water activity in the solution [39,76,77]. However, in our system the difference between water activity at highest and lowest values is trivial ($0.95 \leqslant a_w \leqslant 1$, calculated by PHREEQC). The increased adhesion we observe is unlikely to be a function of decreased water adsorption. As shown by Heuberger et al. [78], secondary hydration forces due to compressed dehydrated ions ("two-stage collective ion dehydration" in high salt concentration) might be more important in modifying the repulsive interaction between contacting asperities than simply water adsorption directly onto the calcite surface. We propose that the increase in pull-off force for increasing salt concentration can be explained by a combination of reduced repulsion (weak secondary hydration [29,36,78–80]) and increased attraction between contacting asperities due to instantaneous ion-ion correlation at high salt concentration [35].

The adhesive interaction energy of rough surfaces is not characterized by the macroscopic, nominal area of contact (Fig. 8), but rather by the actual contact area, which is a function of the distribution of asperities on the contacting surfaces [81,82], and in the first approximation, increases linearly with applied compressive normal stress [83]. For rough surfaces, the area of contact depends on the number, size and height of asperities (see Fig. 1) and surface forces are measured depending on the geometry, density [53,54,84] and height distribution of contacting surfaces [49,58].

For rough, inorganic surfaces, the macroscopic, effective interfacial energy γ may be expressed as the sum of the product of contact-bond strengths, β, and actual area, σ, of all contacting asperities that define the real surface area, both of which may change with time (t) and applied normal load (F_n):

$$\gamma(F_n, t) = \Sigma_i \beta_i(F_n, t)\sigma_i(F_n, t) \qquad (3)$$

For purely elastic processes, the force required to separate two adhesive surfaces will be independent of both time and applied load as long as the macroscopic surface energy on approach equals that on retraction, $\gamma_R = \gamma_A$ (point A to B in Fig. 10). When γ is not constant (Eq. (3)), the measured adhesion force will depend on the maximum applied load at the contact and time, point B to C vs. D to E, Fig. 10.
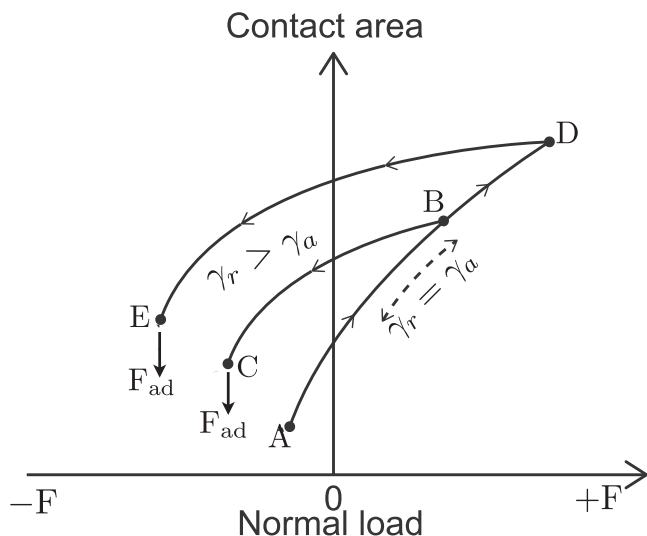
Fig. 10. "Adhesion hysteresis", modified from Israelachvili [28], presenting reversible and irreversible cycles. Upon approach of adhesive surfaces, they jump into contact at A and move along the path to B with increasing normal load. In the case of constant interfacial energy ($\gamma_R = \gamma_A$), unloading follows the same path back to A and the force measured at separation is independent of the maximum applied load. If $\gamma_R > \gamma_A$, separation follows the path from B to C. The measured force of adhesion in this case depends on the maximum applied load (C vs E).

the applied normal stress, indicating that the population of asperities generate the total contact area which differs from nominal surface area of contacting surfaces. In agreement with [24], we measured strong repulsion in low concentration and $CaCO_3$ solutions due to the repulsive hydration forces.

Previous studies suggested that water activity is the key parameter in the strength of calcium carbonate bearing rocks [10,12,24] and single calcite crystals in salt solutions [38]. Based on our measurements, the strengthening process can be explained through progressively weaker secondary hydration and stronger ion-ion correlation forces in NaCl solutions with higher concentration than 100 mM. In addition, we see no indication of consistent flattening of asperities, which could have been related to progressive calcite recrystallization or asperity creep.

Acknowledgments

Here, the contact-bond strength β will be given by the fluid chemistry as discussed above, while F_n determines whether a given contact will be pushed past any repulsive barrier into adhesive contact. Therefore, when repulsive barriers are small enough to be overcome, the number of asperities that make it into adhesive contact, and correspondingly the measured pull-off force will be a function of the applied normal load. This is consistent with what we observe. The time dependence of β takes into account any possible chemical strengthening of asperities that might result from diffusion of ions or slow chemical reactions.

Irreversible changes in σ can take place through nonelastic processes such as twinning [23,85] or breakage of asperities upon pressure, or through stress-induced dissolution and re-precipitation (pressure solution) [29,49,84,86–88] of highly stressed asperities and increase in size of contact area, σ ("asperity creep"). However, all these processes cause a permanent change in the surface topography that would remain present as a different measured pull-off force when lower loads are applied. We observe otherwise; as seen in Fig. 7, the pull-off force returns to the initial value when the setpoint (normal load) is reduced. The slow, non-monotonic change in F_{ad} indicates that there is no consistent flattening of asperities and increase of actual contact area with time. Therefore, we propose that the slow changes in F_{ad} with time may be caused by slow lateral drift or recrystallization.

5. Conclusion

Our measurements show a significant effect of normal load and salinity of the contacting solution on the adhesion of calcite surfaces. We discuss the effect of roughness on pull-off force measurements in NaCl solutions, and categorize it into mechanisms responsible for (1) strengthening the contact-bonds, that is discussed to be mostly due to the combination of weak secondary repulsion and ion-ion correlation forces along with the applied normal stress that generate strong contact-bonds at high salt concentration, and (2) variation in the contact area that is mostly attributed to the local recrystallization of single asperities in a multiple asperity system. The measured pull-off force increases with

References

[1] A.J. Skinner, J.P. LaFemina, H.J.F. Jansen, Am. Mineral. 79 (1994) 205–214.
[2] N.H. de Leeuw, S.C. Parker, J. Phys. Chem. B 102 (1998) 2914–2922.
[3] F. Heberling, T.P. Trainor, J. Lutzenkirchen, P. Eng, M.A. Denecke, D.J. Bosbach, Colloid Interface Sci. 354 (2011) 843–857.
[4] H.A. Lowenstam, Geology 62 (1954) 284–322.
[5] E. Liteanu, C.J. Spiers, Chem. Geol. 265 (2009) 134–147.
[6] K.S. Lackner, C.H. Wendt, D.P. Butt, E.L. Joyce, D.H. Sharp, Energy 20 (1995) 1153–1170.
[7] L. Truche, G. Berger, C. Destrigneville, D. Guillaume, E. Giffaut, Geochim. Cosmochim. Acta 74 (2010) 2894–2914.
[8] M. D'Heur, Mar. Pet. Geol. 1 (1984) 211–238.
[9] R. Risnes, O. Flaageng, Oil Gas Sci. Technol. 54 (1999) 751–758.
[10] T. Heggheim, M. Madland, R. Risnes, T. Austad, J. Petrol. Sci. Eng. 46 (2005) 171–184.
[11] R. Risnes, Phys. Chem. Earth (A) 26 (2001) 53–57.
[12] R. Risnes, H. Haghighi, R.I. Korsnes, O. Natvik, Tectonophysics 370 (2003) 213–226.
[13] R. Hellmann, P. Renders, J. Gratier, R. Guiguet, Water-Rock Interact. (2002) 129–152.
[14] A. Hiorth, L.M. Cathles, M.V. Madland, Transp. Porous Media 85 (2010) 1–21.
[15] M. Megawati, A. Hiorth, M.V. Madland, Rock Mech. Rock Eng. 46 (2012) 1073–1090.
[16] M.V. Madland, A. Hiorth, E. Omdal, M. Megawati, T. Hildebrand-Habel, R.I. Korsnes, S. Evje, L.M. Cathles, Transp. Porous Media 87 (2011) 679–702.
[17] A. Nermoen, R.I. Korsnes, A. Hiorth, M.V. Madland, J. Geophys. Res. 120 (2015) 2935–2960.
[18] R. Risnes, M. Madland, M. Hole, N. Kwabiah, J. Petrol. Sci. Eng. 48 (2005) 21–36.
[19] G. Newman, Soc. Petrol. Eng. 35 (1983) 976–980.
[20] R. Hellmann, J. Gratier, P. Renders, Deformation of chalk by pressure solution, 1996.
[21] P. Delage, C. Schroeder, Y. Cui, Subsidence and capillary effects in chalks, 2008.
[22] E. Liteanu, C.J. Spiers, Chem. Geol. 265 (2009) 134–147.
[23] A. Røyne, J. Bisschop, D.K. Dysthe, J. Geophys. Res. 116 (2011) B04204.
[24] A. Røyne, K.N. Dalby, T. Hassenkam, Geophys. Res. Lett. 42 (2015) 4786–4794.
[25] B. Derjaguin, L. Landau, Prog. Surf. Sci. 43 (1941) 1–4.
[26] E. Verwey, J.T.G. Overbeek, Elsevier, Amsterdam 1948.
[27] J. Overbeek, E.J.W. Verwey, Theory of the Stability of Lyophobic Colloids, Elsevier, 1948.
[28] J.N. Israelachvili, third ed., Intermolecular and Surface Forces, vol. 1, Elsevier, 2011.
[29] Y. Diao, R.M. Espinosa-Marzal, Proc. Natl. Acad. Sci. USA 113 (2016) 12047–12052.
[30] J.N. Israelachvili, R.M. Pashley, Nature 306 (1983) 249–250.
[31] Z. Zachariah, R.M. Espinosa-Marzal, N.D. Spencer, M.P. Heuberger, Phys. Chem. Chem. Phys. 18 (2016) 24417–24427.
[32] J. Chun, C.J. Mundy, G.K. Schenter, J. Phys. Chem. B 119 (2015) 5873–5881.

[33] M. Ricci, P. Spijker, F. Stellacci, J.F. Molinari, K. Voitchovsky, Langmuir 29 (2013) 2207–2216.
[34] L. Guldbrand, B. Jönsson, H. Wennerström, P. Linse, J. Chem. Phys. 80 (1984) 2221–2228.
[35] B. Joensson, H. Wennerstroem, A. Nonat, B. Cabane, Langmuir 20 (2004) 6702–6709.
[36] S.H.J. Donaldson, A. Royne, K. Kristiansen, M.V. Rapp, S. Das, M.A. Gebbie, D.W. Lee, P. Stock, M. Valtiner, J. Israelachvili, Langmuir 31 (2015) 2051–2064.
[37] S. Pourchet, I. Pochard, F. Brunel, D. Perrey, Cem. Concr. Res. 52 (2013) 22–30.
[38] F. Rostom, A. Royne, D.K. Dysthe, F. Renard, Tectonophysics 583 (2013) 68–75.
[39] M. Kohns, M. Schappals, M. Horsch, H. Hasse, J. Chem. Eng. Data 61 (2016) 4068–4076.
[40] M.J. Blandamer, J.B. Engberts, P.T. Gleeson, J.C. Reis, Chem. Soc. Rev. 34 (2005) 440–458.
[41] H.J. Butt, K. Graf, M. Kappl, Physics and Chemistry of Interfaces, Wiley, 2003.
[42] E. Ruiz-Agudo, M. Kowacz, C.V. Putnis, A. Putnis, Geochim. Cosmochim. Acta 74 (2010) 1256–1267.
[43] T. Foxall, G.C. Peterson, H.M. Rendall, A.L.J. Smith, Chem. Soc. Faraday Trans. 1 75 (1979) 1034–1039.
[44] S.L.S. Stipp, Geochim. Cosmochim. Acta 63 (1999) 3121–3131.
[45] U. Ulusoy, C. Hiçyilmaz, M. Yekeler, Chem. Eng. Process. 43 (2004) 1047–1053.
[46] U. Ulusoy, M. Yekeler, Chem. Eng. Process. 44 (2005) 555–563.
[47] S.-Y. Chen, Y. Kaufman, K. Kristiansen, D. Seo, A.M. Schrader, M.B. Alotaibi, H.A. Dobbs, N.A. Cadirov, J.R. Boles, S.C. Ayirala, J.N. Israelachvili, A.A. Yousef, Energy Fuels 31 (2017) 8925–8941.
[48] E. Thormann, Curr. Opin. Colloid Interface Sci. 27 (2017) 18–24.
[49] D.F. Parsons, R.B. Walsh, V.S.J. Craig, Chem. Phys. 140 (2014) 164701.
[50] M. Valtiner, X. Banquy, K. Kristiansen, G.W. Greene, J.N. Israelachvili, Langmuir 28 (2012) 13080–13093.
[51] E.M. Hoek, G.K.J. Agarwal, Colloid Interface Sci. 298 (2006) 50–58.
[52] J.F.L. Duval, F.A.M. Leermakers, H.P.V. Leeuwen, Langmuir 20 (2004) 5052–5065.
[53] S. Bhattacharjee, C.H. Ko, M. Elimelech, Langmuir 14 (1998) 3365–3375.
[54] L. Suresh, J.Y. Walz, Colloids Interface Sci. 183 (1996) 199–213.
[55] Z. Adamczyk, P. Weroński, Adv. Colloid Interface Sci. 83 (1999) 137–226.
[56] B.N.J. Persson, Surf. Sci. Rep. 61 (2006) 201–227.
[57] B.N. Persson, M. Scaraggi, J Chem Phys 141 (2014) 124701.
[58] N. Eom, D.F. Parsons, V.S.J. Craig, J. Phys. Chem. B 121 (2017) 6442–6453.
[59] J.A. Brant, A.E. Childress, Environ. Eng. Sci. 19 (2004) 413–427.
[60] S. Stipp, W. Gutmannsbauer, T. Lehmann, Am. Mineral. 81 (1996) 1–8.
[61] S.L.S. Stipp, J. Konnerup-Madsen, K. Franzreb, A. Kulik, H.J. Mathieu, Nature 396 (1998) 356–359.
[62] J. Dziadkowiec, S. Javadi, J.E. Bratvold, O. Nilsen, A. Royne, Langmuir (2018).
[63] Y. Levenson, S. Emmanuel, Geochem. Perspect. Lett. (2017) 133–141.
[64] X. Liu, W. Yan, E.H. Stenby, E. Thormann, Energy Fuels 30 (2016) 3986–3993.
[65] S.J. Fathi, T. Austad, S. Strand, Water-Based Enhanced Oil Recovery (EOR) by Smart Water in Carbonate Reservoirs, 2012.
[66] S.J. Fathi, T. Austad, S. Strand, Energy Fuels 24 (2010) 2514–2519.
[67] H.-J. Butt, B. Cappella, M. Kappl, Surf. Sci. Rep. 59 (2005) 1–152.
[68] M. Farshchi-Tabrizi, M. Kappl, Y. Cheng, J. Gutmann, H.J. Butt, Langmuir 22 (2006) 2171–2184.
[69] J.L. Hutter, J. Bechhoefer, Rev. Sci. Instrum. 64 (1993) 1868–1873.
[70] D.L. Parkhurst, User's guide to Phreeqc – A computer program for speciation, reaction-path, advective-transport, and inverse geochemical calculations, Report, 1995.
[71] S.L.S. Stipp, C.M. Eggleston, B.S. Nielsen, Geochim. Coesmochim. Acta 58 (1994) 3023–3033.
[72] M. Wolthers, L. Charlet, P.V. Cappellen, Am. J. Sci. (2008).
[73] A.M. Smith, A.A. Lee, S. Perkin, J. Phys. Chem. Lett. 7 (2016) 2157–2163.
[74] M. Valtiner, K. Kristiansen, G.W. Greene, J.N. Israelachvili, Adv. Mater. 23 (2011) 2294–2299.
[75] R.M. Pashley, J.N. Israelachvili, Colloid Interface Sci. 97 (1984) 446–455. https://www.sciencedirect.com/science/article/pii/0021979784903163.
[76] S.M. Mutisya, A. Kirch, J.M. de Almeida, V.M. Sánchez, C.R. Miranda, J. Phys. Chem. C 121 (2017) 6674–6684.
[77] D. Di Tommaso, E. Ruiz-Agudo, N.H. de Leeuw, A. Putnis, C.V. Putnis, Phys. Chem. Chem. Phys. 16 (2014) 7772–7785.
[78] M.P. Heuberger, Z. Zachariah, N.D. Spencer, R.M. Espinosa-Marzal, Phys. Chem. Chem. Phys. 19 (2017) 13462–13468.
[79] S. Marčelja, Curr. Opin. Colloid Interface Sci. 16 (2011) 579–583.
[80] R.M. Espinosa-Marzal, T. Drobek, T. Balmer, M.P. Heuberger, PCCP 14 (2012) 6085–6093.
[81] K.N.G. Fuller, D. Tabor F.R.S, Proc. Roy. Soc. Lond. A. Math. Phys. Sci. 345 (1975) 327–342, https://doi.org/10.1098/rspa.1975.0138.
[82] P. Prokopovich, S. Perni, Langmuir 26 (2010) 17028–17036.
[83] J.A. Greenwood, J.B.P. Williamson, Proc. Roy. Soc. Lond. Ser. A Math. Phys. Sci. 295 (1966) 300–319.
[84] X. Huang, S. Bhattacharjee, E.M. Hoek, Langmuir 26 (2010) 2528–2537.
[85] F.P. Bowden, R.E. Cooper, Nature (1962) 1091–1092.
[86] N. Alcantar, J. Israelachvili, J. Boles, Geochim. Cosmochim. Acta 67 (2003) 1289–1304.
[87] D. Croizé, F. Renard, K. Bjørlykke, D.K. Dysthe, J. Geophys. Res. (2010) 115.
[88] F. Renard, S. Beauprêtre, C. Voisin, D. Zigone, T. Candela, D.K. Dysthe, J.-P. Gratier, Earth Planet. Sci. Lett. (2012) 20–34.